Electron- and positron-impact ionization of inert gases

R. I. Campeanu
Department of Physics and Astronomy, York University, Toronto, Canada M3J 1P3

H. R. J. Walters
Centre for Theoretical Atomic, Molecular, and Optical Physics, School of Mathematics and Physics, Queen's University, Belfast BT7 1NN, United Kingdom

Colm T. Whelan*
Department of Physics, Old Dominion University, Norfolk, Virginia 23539, USA

(Received 6 August 2017; revised manuscript received 26 February 2018; published 8 June 2018)

Triple-differential cross sections (TDCS) are presented for the electron and positron impact ionization of inert gas atoms in a range of geometries where a number of significant few body effects compete to define the shape of the TDCS. Using both positrons and electrons as projectiles has opened up the possibility of performing complementary studies which could effectively isolate competing interactions which cannot be separately detected in an experiment with a single projectile. A comparison is presented between theory and the recent experiments of [Gavin, deLucio, and DuBois, Phys. Rev. A **95**, 062703 (2017)] for $e^{\pm}$ and contrasted with the results from earlier electron experiments. For the special case of xenon($5p$), cross sections are presented for both electron- and positron-impact ionization in kinematics where the electron case appears well understood. The kinematics are then varied in order to focus on the possible role of distortion, exchange, and target wave-function effects.

DOI: 10.1103/PhysRevA.97.062702

I. INTRODUCTION

Coincidence techniques are a powerful way of studying atomic collision processes. Using them much has been learned about the subtleties of the interactions in collisions between photons, ions, and electrons with atomic and molecular targets. More recent pioneering work using antimatter projectiles, e.g., [1,2], has opened up the possibility of performing complementary experiments which could effectively isolate competing interactions which cannot be separately detected in an experiment with a single projectile. Such experiments [3,4] have recently been performed for electron and positron impact of Ar($3p$) [5] at an impact energy of 1 keV, which is sufficiently high that annihilation and capture effects for the positron can be safely neglected. A coincidence experiment places a much more severe test on theory than less differential measurements, and while there have been some interesting experimental and theoretical results presented for double-differential cross sections [6–10], the focus here will be exclusively on the triple-differential cross section. The experiment of [4] suffered from the size of the errors that had to be tolerated; nevertheless, suitably averaged distorted-wave Born approximation (DWBA) calculations [11] behaved reasonably well in describing these results. The experimental program is under development, and there is a need for reliable fully quantum-mechanical calculations to help give an impetus to this effort. Also, the new experiments directly compare e^- and e^+ impact ionization in the same kinematics. For the electron case there is an abundance of high-quality experimental data, and if we are to understand how and why the positron case differs from the electron case, we need an approach that works well for the latter for the targets (heavy inert gases) and kinematics (coplanar asymmetric) favored by current measurements. Some earlier theoretical studies of the triple-differential cross sections (TDCSs) for positron scattering may be found in [12–14], but these calculations were restricted to atomic hydrogen. Our aim here is to treat multielectron targets. Here the DWBA approach has been successful in describing $(e^-,2e^-)$ experiments [15–25]. Therefore, it seems reasonable to use it to explore positron-impact ionization. A virtue of the DWBA is that its relative simplicity enables us to isolate the separate contributions to ionization of effects such as exchange and distortion. In its basic form the DWBA does not take account of postcollisional interactions (PCI) between the scattered projectile (electron or positron) and the ejected electron. However, modifying the DWBA by the addition of a Gamov factor gives a reasonable way of assessing the importance of PCI. Atomic units ($\hbar = e = m_e = 1$) are used throughout.

II. COINCIDENCE MEASUREMENTS

In a coincidence experiment a projectile of momentum $\mathbf{k}_0$ and energy E_0 impinges on a target atom and ionizes it. The ejected electron and scattered projectile are detected with their angles and energies resolved. The momentum vectors of the scattered projectile $\mathbf{k}_1$ and the ejected electron $\mathbf{k}_2$ form a plane, and thus we can define all possible kinematics by the set $(k_0,k_1,k_2,\Phi,\theta_1,\theta_2)$, where Φ defines the angle $\mathbf{k}_0$ makes

*cwhelan@odu.edu

 ©2018 American Physical Society

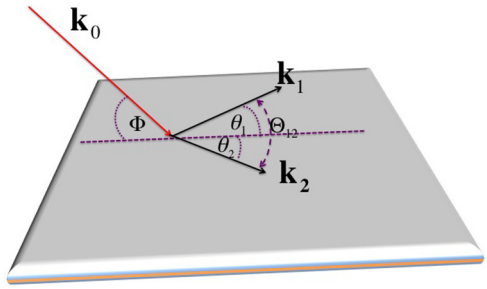

FIG. 1. The fast incoming projectile has momentum $\mathbf{k}_0$ and energy E_0 and comes in at an angle Φ with respect to the plane in which the two final-state particles are detected at angles θ_1,θ_2 with respect to the projection of the incoming direction on their plane. $\Phi = 0^\circ$ corresponds to coplanar geometry, $\Phi = 90^\circ$ to perpendicular plane geometry, and Θ_{12} is the angle between the two detected particles.

to the plane of detection, the "gun angle" (see Fig. 1). Such a measurement is kinematically complete and is ideal for exploring subtle collisional effects which would be swamped by more robust interactions in a less differential measurement.

III. THEORY

A. Electron impact

The distorted-wave Born approximation has been applied to electron-impact ionization for quite some time, the first detailed account being given by [26]; the version we use here is in essential features the same with some refinements. For a full discussion of the approximation, its strengths, weaknesses, and our computational implementation see [19,24]. For the electron-impact ionization of the n,l orbital of an inert gas atom, the TCDS, after summing over all final and averaging over all initial spin states, is given by

$$\frac{d^3\sigma^{\rm DWBA}}{d\Omega_1 d\Omega_2 dE} = 2(2\pi)^4 \frac{k_1 k_2}{k_0} \sum_{m=-l}^{l} [|f_{nlm}|^2 + |g_{nlm}|^2 - {\rm Re}(f^*_{nlm} g_{nlm})], \quad (1)$$

where

$$f_{nlm}(\mathbf{k}_1,\mathbf{k}_2) = \langle \chi^-(\mathbf{k}_1,\mathbf{r}_1)\chi^-(\mathbf{k}_2,\mathbf{r}_2)| \frac{1}{\|\mathbf{r}_1 - \mathbf{r}_2\|} \times |\chi_0^+(\mathbf{k}_0,\mathbf{r}_1)\psi_{nlm}(\mathbf{r}_2)\rangle,$$
$$g_{nlm}(\mathbf{k}_1.\mathbf{k}_2) = \langle \chi^-(\mathbf{k}_1,\mathbf{r}_2)\chi^-(\mathbf{k}_2,\mathbf{r}_1)| \frac{1}{\|\mathbf{r}_1 - \mathbf{r}_2\|} \times |\chi_0^+(\mathbf{k}_0,\mathbf{r}_1)\psi_{nlm}(\mathbf{r}_2)\rangle. \quad (2)$$

Here χ_0^+ is the distorted wave calculated in the static-exchange potential of the atom, and the χ^-'s are distorted waves calculated in the static-exchange potential of the ion and then orthogonalized to ψ_{nlm}. These are normalized to a δ function, i.e.,

$$\langle \chi^\pm(\mathbf{k},\mathbf{r})|\chi^\pm(\mathbf{k}',\mathbf{r})\rangle = \delta(\mathbf{k} - \mathbf{k}'). \quad (3)$$

For the target wave functions we use the Hartree-Fock orbitals given in [27]. In the approximation (2) the electron-electron interaction occurs exactly once and no account is taken of PCI between the two final-state electrons. In our calculations below, the full nonlocal exchange potential is not used but rather a localized version [19,28–31] is employed. Its use greatly simplifies the static-exchange calculations in that one needs only solve differential equations rather than integrodifferential equations. Because we treat each of the exiting electrons as moving in the field of a spin-$\frac{1}{2}$ ion, there is an inherent ambiguity in the choice of exchange potential in the final channels—we could chose it to be singlet or triplet [19,32]. For most energies there is little or no difference between results calculated with the singlet or triplet potentials [19,31], but at low energies there is a weakness in the singlet form: for some energies it can become complex. A method has been proposed in [29] to make the potential real again if this happens, but this method results in a discontinuous singlet potential and generally gives results in poorer agreement with experiment than the equivalent triplet calculation (see [19,25]). The neglect of PCI could be important. To take some account of it a Gamow factor N_{e-e-} [15,33] is sometimes employed,

$$\frac{d^3\sigma^{\rm PCI}}{d\Omega_1 d\Omega_2 dE} = N_{e-e-} \frac{d^3\sigma^{\rm DWBA}}{d\Omega_1 d\Omega_2 dE}, \quad (4)$$

where

$$N_{e-e-} = \frac{\gamma}{e^\gamma - 1} \quad (5)$$

with

$$\gamma = \frac{2\pi}{\|\mathbf{k}_1 - \mathbf{k}_2\|}. \quad (6)$$

The Gamov factor is related to the analytic ansatz approximation of Brauner, Briggs, and Klar (BBK) [12]. The essence of the BBK approximation is to assume that the full three-body wave function could be approximated by three two-body wave functions corresponding to the three final-state particles all independently acting in pairs. The approach has the appealing advantage of treating each two-body system in a symmetric way. The N_{e-e-} factor comes from the Coulomb wave representing the two-body interaction between the two outgoing electrons [13,34]. The BBK approximation tends to give a reasonable representation of the shape of the TDCS but unfortunately yields only a poor representation of the absolute size of the cross section and is difficult to apply to multielectron targets [35,36]. Nevertheless, the N_{e-e-} factor tends to give the dominant angular behavior of the TDCS at low energies and it does correctly force the cross section to go to zero when $\mathbf{k}_1 = \mathbf{k}_2$. However, the overall normalization is lost. To ameliorate this it is usual to have N_{e-e-} normalized so that it is fixed to 1 when the angle between $\mathbf{k}_1$ and $\mathbf{k}_2$ is 180°.

A modified version of the N_{e-e-} factor has been put forward by Ward and Macek [37]. These authors suggested replacing N_{e-e-} by

$$M_{e-e-} = N_{e-e-}|{}_1F_1(-i\nu_3, 1, -2ik_3 r_{3av})|, \quad (7)$$

where

$$k_3 = \frac{1}{2}\|\mathbf{k_1} - \mathbf{k_2}\|,$$
$$\nu_3 = -\frac{1}{\|\mathbf{k_1} - \mathbf{k_2}\|}, \quad (8)$$
$$r_{3av} = \frac{3}{\epsilon}\left[\frac{\pi}{4\sqrt{(3)}}\left(1 + \frac{0.627}{\pi}\sqrt{\epsilon}\ln\epsilon\right)\right]^2,$$

with ϵ being the total energy of the two emerging electrons. The parameter r_{3av} is chosen by the requirement that the $M_{e^-e^-}$ factor reproduce the Wannier behavior and thus it is hoped to correctly "normalize" $N_{e^-e^-}$.

The use of $N_{e^-e^-}$, or indeed $M_{e^-e^-}$ for that matter, is a relatively crude way of including PCI effects and it is only really useful very close to threshold [19]. The use of a somewhat cruder approximation than the DWBA can be informative. The simplest possible approximation to the TDCS is to neglect the exchange amplitude g_{nlm} and to assume that the impulsive interaction between the incident and target electron is dominant, and that we can represent the incoming and outgoing particles as plane waves corresponding to classical straight-line trajectories. This gives us the plane-wave impulse approximation (PWIA) (see [24,38]):

$$f_{nlm}^{\mathrm{PWIA}}(\mathbf{k}_1,\mathbf{k}_2) = -\frac{1}{(2\pi)^{9/2}}\int e^{-i(\mathbf{k}_1\cdot\mathbf{r}_1)}e^{-i(\mathbf{k}_2\cdot\mathbf{r}_2)}\left[\frac{1}{r_{12}}\right] \times \psi_{nlm}(\mathbf{r}_2)e^{i\mathbf{k}_0\cdot\mathbf{r}_1}d^3r_1d^3r_2. \tag{9}$$

The PWIA does not contain any form of multiple scattering or exchange. The initial and final wave functions are not eigenfunctions of the same Hamiltonian and thus not orthogonal, which leads to the cross section having the wrong asymptotic behavior as the momentum transfer q goes to zero. Its principal merit is that the explicit dependence of the TDCS on the target wave function is immediately apparent.

Returning to (9) and making use of the well-known Bethe relation [39]

$$\int d^3r_1 e^{i(\mathbf{k}_0-\mathbf{k}_1)\cdot\mathbf{r}_1}\frac{1}{\|\mathbf{r}_1-\mathbf{r}_2\|} = \frac{4\pi}{q^2}e^{i(\mathbf{q}\cdot\mathbf{r}_2)}, \tag{10}$$

where $\mathbf{q} = \mathbf{k_0} - \mathbf{k}_1$ is the momentum transfer vector, we find

$$f_{nlm}^{\mathrm{PWIA}}(\mathbf{k}_1,\mathbf{k}_2) = \frac{-2}{(2\pi q)^2}\left[\frac{1}{(2\pi)^{3/2}}\int d^3r e^{i(\mathbf{k}_0-\mathbf{k}_1-\mathbf{k}_2)\cdot\mathbf{r}}\psi_{nlm}(\mathbf{r})\right] = \frac{-2}{(2\pi q)^2}\phi_{nlm}(\mathbf{k}_{\mathrm{recoil}}), \tag{11}$$

where

$$\mathbf{k}_{\mathrm{recoil}} = \mathbf{k}_0 - \mathbf{k}_1 - \mathbf{k}_2\,, \tag{12}$$

and $\phi_{nlm}(\mathbf{k}_{\mathrm{recoil}})$ is the wave function in momentum space. The integral in (11) may be evaluated by substituting the usual radial form

$$\psi_{nlm}(\mathbf{r}) = R_{nl}(r)Y_{lm}(\hat{\mathbf{r}}) \tag{13}$$

and expanding the plane wave in spherical harmonics to find that

$$f_{nlm}^{\mathrm{PWIA}} = \frac{-2}{(2\pi q)^2}\left\{\frac{4\pi i^l}{(2\pi)^{3/2}}\left[\int_0^\infty r^2dr\,R_{\mathrm{nl}}j_l(k_{\mathrm{recoil}}r)Y_{lm} \times (\hat{\mathbf{k}}_{\mathrm{recoil}})\right]\right\} = \frac{-2}{(2\pi q)^2}F_{nl}(k_{\mathrm{recoil}})Y_{lm}(\hat{\mathbf{k}}_{\mathrm{recoil}}). \tag{14}$$

Note that F_{nl} does not depend on the magnetic quantum number m. Since ψ_{nlm} is normalized to unity it follows that

$$\int_0^\infty p^2|F_{nl}(p)|^2dp = 1. \tag{15}$$

The probability that the absolute value of the momentum lies between p and $p+dp$ is given by $p^2|F_{n,l}(p)|^2dp$. Substituting in (1) we have

$$\frac{d^3\sigma^{\mathrm{PWIA}}}{d\Omega_1 d\Omega_2 dE} = \frac{8k_1k_2}{q^4k_0}\frac{(4\pi)^2}{(2\pi)^3}\left|\int_0^\infty drr^2R_{nl}(r)j_l(k_{\mathrm{recoil}}r)\right|^2 \times \sum_{m=-l}^{l}Y_{lm}^*(\hat{\mathbf{k}}_{\mathrm{recoil}})Y_{lm}(\hat{\mathbf{k}}_{\mathrm{recoil}}), \tag{16}$$

but from Unsöld's theorem [40],

$$\sum_{m=-l}^{l}Y_{lm}^*(\hat{\mathbf{k}}_{\mathrm{recoil}})Y_{lm}(\hat{\mathbf{k}}_{\mathrm{recoil}}) = \frac{2l+1}{4\pi} \tag{17}$$

and hence,

$$\frac{d^3\sigma^{\mathrm{PWIA}}}{d\Omega_1 d\Omega_2 dE} = (2l+1)\frac{k_1k_2}{k_0q^4}\frac{4}{\pi^2}\left[\int_0^\infty r^2R_{nl}(r)j_l(k_{\mathrm{recoil}}r)\right]^2. \tag{18}$$

Thus the triple-differential cross section separates into the product of two factors. The one in the square bracket in (18) depends purely on the target and the second, which contains the q^{-4} factor, looks like the classical Rutherford scattering term. Clementi and Roetti [27] give analytic fits to the Hartree-Fock spatial orbitals in terms of an expansion over Slater orbitals of the general form

$$\chi_{nlm} = N(n,\alpha)r^{n-1}e^{-\alpha r}Y_{lm}(\theta,\phi) \tag{19}$$

where

$$N(n,\alpha) = \frac{(2\alpha)^{n+\frac{1}{2}}}{[(2n)!]^{\frac{1}{2}}}. \tag{20}$$

Using these functions $F_{nl}(k_{\mathrm{recoil}})$ can then be reduced to a sum over integrals of the form

$$I_W(\beta,m,l,k_{\mathrm{recoil}}) = \int_0^\infty e^{-\beta r}r^m\,j_l(k_{\mathrm{recoil}}r)dr. \tag{21}$$

Such integrals admit an analytic solution [41]. From (14) it follows that the TDCS in the PWIA will have a zero whenever $F_{nl}(k_{\mathrm{recoil}})$ has a node. In Fig. 2 we plot $|F_{51}|^2$ for xenon. It will be helpful to consider the nodes of the momentum space wave function: the first node is at the origin, a second node which corresponds to an exact zero in the plane-wave cross section occurs when $k_{\mathrm{recoil}} \approx 2.94$ a.u., and there is a further minimum at $k_{\mathrm{recoil}} \approx 7.25$ a.u. The first maximum in $|F_{5,1}|^2$ is at $k \approx 0.578$ a.u. For $k > 2.0$ a.u. the amplitude of the function is very small, so in order to explicitly show the nodes we have plotted it on both a linear and a log scale. Let us first consider the zero at the Bethe ridge point $k_{\mathrm{recoil}} = 0$. Depending on the impact and binding energies, such a zero may or may not be possible. In coplanar asymmetric geometry where one particle is detected at some fixed anticlockwise angle θ_1 and the TDCS is given as a function of the clockwise measured angle θ_2, then conservation of energy and the Bethe point

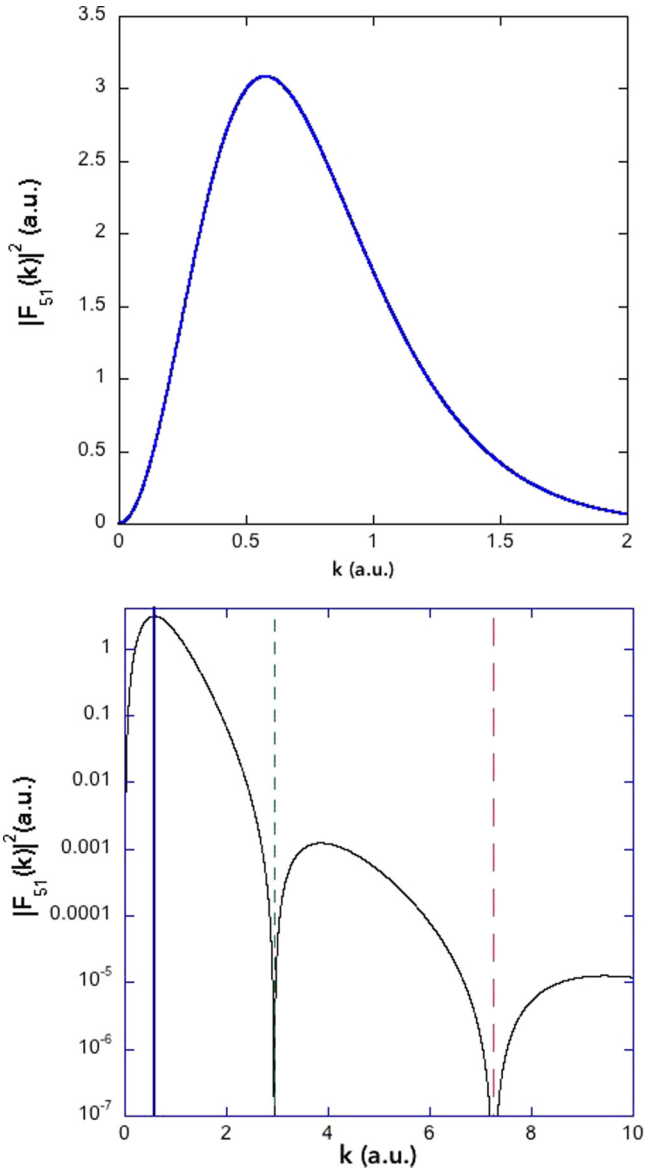

FIG. 2. The function $|F_{51}(k)|^2$ plotted for xenon. In the left panel we use a linear scale. In the right we use a log scale where the solid blue vertical line is $k = 0.578$, the short dashed green line is $k = 2.94$ a.u., and the long dashed red line is $k = 7.25$ a.u.

give us

$$\begin{aligned} k_0^2 &= k_1^2 + k_2^2 + 2I \\ \mathbf{k}_0 - \mathbf{k}_1 &= \mathbf{k}_2 \\ \Rightarrow k_0^2 + k_1^2 - 2k_1k_0\cos\theta_1 &= k_2^2 \\ \Rightarrow k_0^2 + k_1^2 - 2k_1k_0\cos\theta_1 &= k_0^2 - 2I - k_1^2 \\ \Rightarrow \cos\theta_1 &= \frac{k_1^2 + I}{k_1k_0}. \end{aligned} \tag{22}$$

Even if it is not kinematically possible to reach the Bethe point itself, we will still have a minimum in the TDCS if k_{recoil} is smaller than the $k = k_{\max}$ which gives the first maximum in $F_{n,l}(k)$. The PWIA is too crude an approximation for almost all electron and positron experiments. A somewhat better approximation is the first Born approximation (FBA), in which we continue to ignore the exchange term and use plane waves for the incident and scattered particles but treat the wave function of the ejected electron as a continuum state of the ion. The Bethe integral relation can still be employed and the TDCS is symmetric about the direction of momentum transfer. As a consequence of the orthogonality between initial and final ejected electron states, the FBA has the correct asymptotic form as $q \to 0$.

B. Positron impact

We will again use the DWBA, (1) to (2). In this case there is no exchange amplitude $g_{nlm} = 0$, and the distorted waves $\chi_0^+(\mathbf{k}_0, \mathbf{r}_1)$ and $\chi^-(\mathbf{k}_1, \mathbf{r}_1)$ for the positron are generated in the static potential of the atom(ion) for positron impact (i.e., minus the static potential for electron impact). The distorted wave $\chi^-(\mathbf{k}_2, \mathbf{r}_2)$ for the slow ejected electron is orthogonalized to the bound state. There is now no ambiguity in the choice of exchange potential. The ground state of our targets is spin singlet ($S = 0$) and therefore the ejected wave function must be calculated in the singlet static-exchange potential. To estimate PCI we can make use of a Gamov function again but where now we change the sign of γ in (5),

$$N_{e+e-} = \frac{\Gamma}{e^{\Gamma} - 1} \tag{23}$$

with

$$\Gamma = -\frac{2\pi}{\|\mathbf{k}_1 - \mathbf{k}_2\|}. \tag{24}$$

In a number of earlier calculations, including our own [11], the M_{e+e-} [37] factor was used. In their original derivation Ward and Macek assumed that at threshold both exiting particles (electrons in their case) preferentially moved at 180° to each other, which is consistent with the Wannier model for threshold electron-impact ionization. This will not apply in the positron case. Furthermore, we know [25] that the DWBA + M_{e-e-} gives poor agreement with the absolute experiments of [42,43] at 1 and 2 eV above threshold for the electron-impact ionization of helium. DWBA + N_{e-e-} with N_{e-e-} normalized to 1 at $\Theta_{12} = 180°$ is in accord with both the shape and absolute size of these experiments. We will therefore only make use of Gamov factors N_{e-e-} and N_{e+e-} in the calculations presented below. We will adopt the same normalization for both positron and electron collisions, i.e., we will normalize $N_{e-e-} = 1$,for $\Theta_{12} = 180°$, $N_{e+e-} = 1$,for $\Theta_{12} = 180°$. Neither the PWIA nor the FBA include exchange or postcollisional interaction between the exiting particles and thus they will return the same TDCS for electron and positron scattering.

IV. RESULTS

A. Argon($3p$)

In Fig. 3 we show a comparison between our calculations (DWBA, DWBA with $N_{e^{\pm}e^-}$) and the recent experiments of [3]. The experiments are relative, and we have averaged our calculations over the experimental uncertainties of ±10 eV in the energy and ±0.5° in θ_1. Both the electron and positron results show a similar pattern and reasonable shape agreement

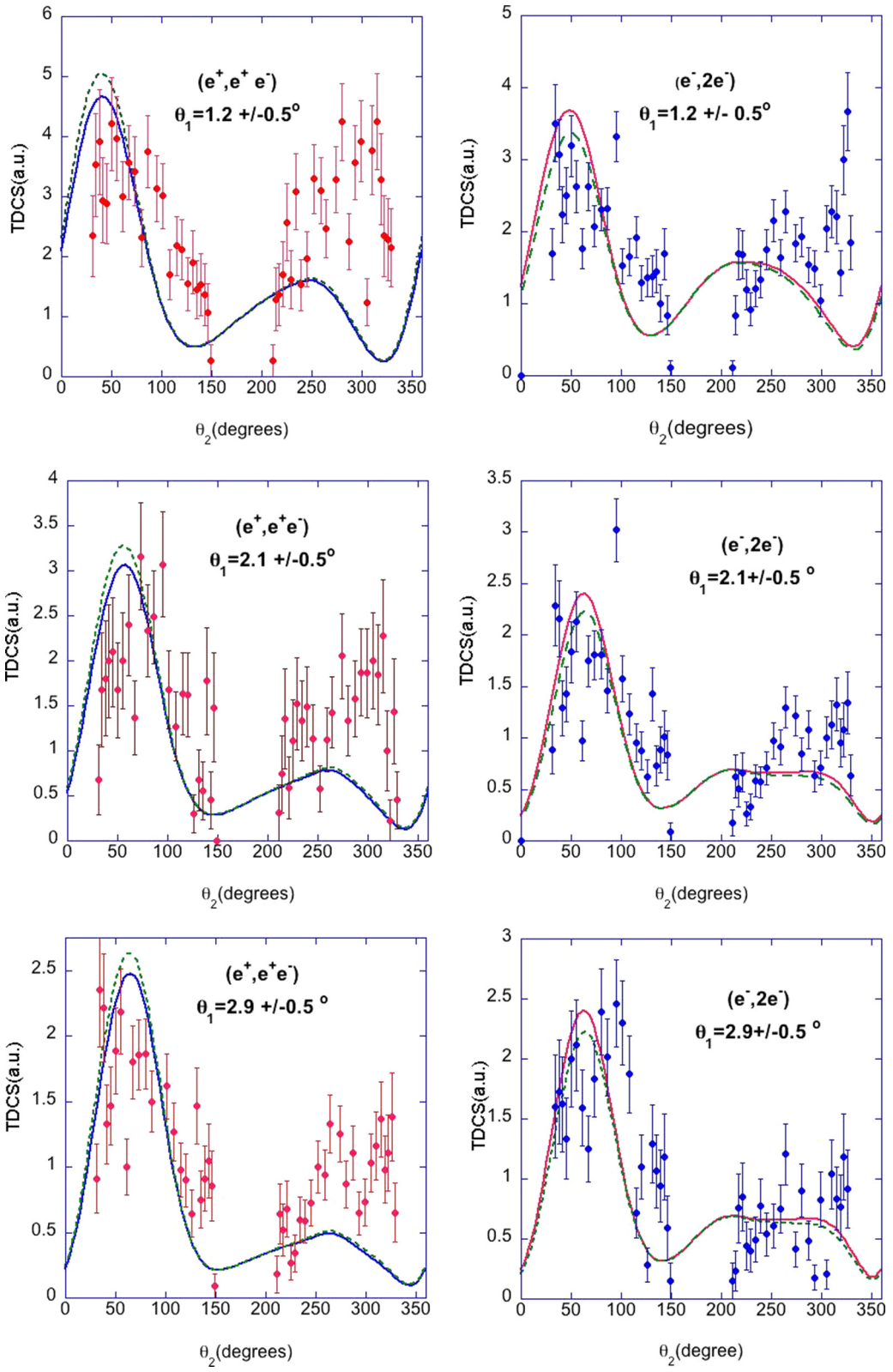

FIG. 3. Triple-differential cross sections for the electron- and positron-impact ionization of Ar($3p$), $E_0 = 1$ keV, $E_2 = 26 \pm 10$ eV, the scattering angle displayed in the individual panels. The positron results are on the left, the electron on the right. Also shown, solid line, DWBA, and dashed line, DWBA+N_{ee} calculations. Experiment [3] was relative and was normalized to give the best visual fit to the DWBA.

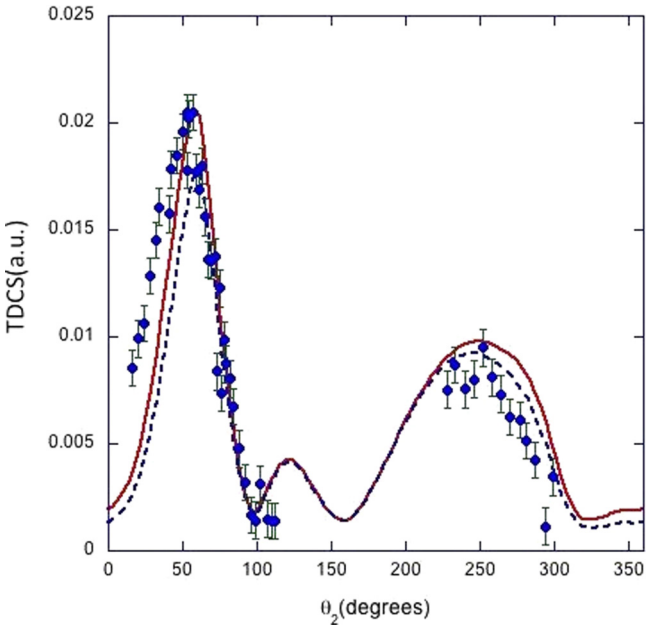

FIG. 4. Triple-differential cross sections for the electron-impact ionization of Ar($3p$), $E_0 = 1015.8$ eV, $E_2 = 120$ eV, $\theta_1 = 8^\circ$. Experimental data from [44], theory: DWBA, solid line, DWBA+N_{ee}, dashed, experiment was relative and normalized to give best visual fit to theory.

with the measurements in the binary direction, but the experimental results tend to overshoot theory in the recoil region and there is an intimation of additional structure in the recoil direction.

There have been quite a number of electron-impact ionization experiments on argon [44–48], but not, to our knowledge, in these precise kinematics of Fig. 3. In Fig. 4 we show a comparison between our calculations and the experiments of [44]. Generally, agreement is good and there is no evidence of any structure in the recoil direction. In [20] experimental results were presented for krypton($4p$) and xenon($5p$) in kinematics which mimic those considered here. In Fig. 5 we compare with these measurements. The agreement is reasonable, and while the theoretical results tend to overestimate the size of the recoil to binary ratio in xenon, there is no structure in the recoil direction. In all our calculations PCI, as incorporated by the $N_{e^\pm,e^-}$ factors, makes only a little difference to the shape, and since all the experiments are relative it is not clear how its influence could be distinguished. Given the amount and quality of experimental data for $(e,2e)$ on argon and the experimental challenges faced in measuring electron and positron-impact ionization in the same experimental device, we are inclined to the view that there is some systematic experimental issue in the measurements of [1] and that the DWBA offers the most practical way of giving direction and guidance to the evolving experimental program. In the next section we focus on xenon targets.

B. Xe($5p$)

Let us first consider the $(e,2e)$ experiments of [20]. These measurements were in coplanar asymmetric geometry, which is ideal for this investigation since we can reasonably hope to avoid the complicating effects of positronium formation and annihilation. The target was xenon at an impact energy of 1.032 keV, with $E_1 = 1$ keV, $E_2 = 20$ eV. In Fig. 6 we show DWBA results at $\theta_1 = 2.5^\circ$ and $\theta_1 = 8^\circ$. Agreement between experiment and the DWBA is encouraging in both cases. There is a local minimum in the binary peak in the direction of momentum transfer at 8°, which is absent in the 2.5° case. Returning to the analysis given above in (22), we see that the Bethe region ($k_{\rm recoil} < k_{\rm max}$) is accessible in the former case but not in the latter, and thus the 8° kinematics is sensitive to the p nature of the target wave function, while the 2.5° experiment is not. PCI, as manifested through the $N_{e^-e^-}$ factor, makes only a little difference. We have calculated the TDCS for positron-impact ionization in the same kinematics. The measurements discussed in this paper are all relative, and given the challenges facing experiment, it would seem unlikely that absolute cross sections will be available in the near future. It is

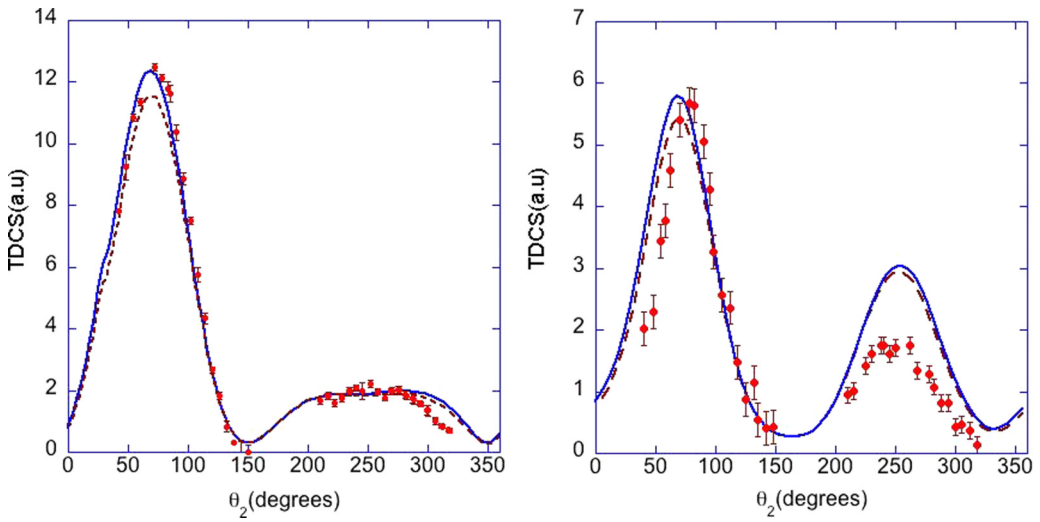

FIG. 5. Triple-differential cross sections for the electron-impact ionization of Kr($4p$) (left panel) and Xe($5p$) (right panel), $E_1 = 1$ keV, $E_2 = 20$ eV, $\theta_1 = 8^\circ$. Experiment from Ref. [20] theory: DWBA solid line, and DWBA+N_{ee} dashed line.

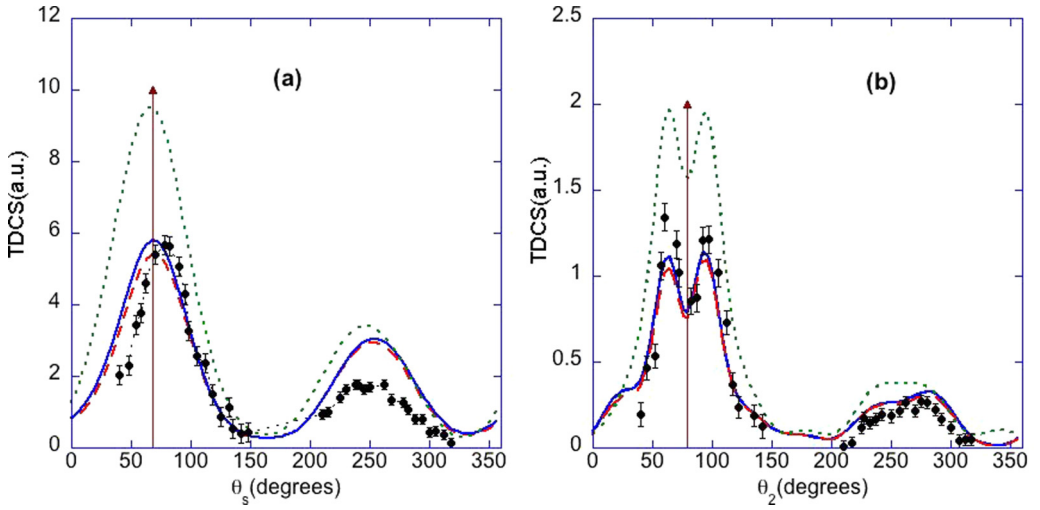

FIG. 6. TDCS for the electron-impact ionization of Xe($5p$), $E_0 = 1.032$ keV, $E_1 = 1$ keV, $E_2 = 20$ eV for (a) $\theta_1 = 2.5^\circ$, (b) $\theta_1 = 8^\circ$. Experiment is from [20]. Curves: DWBA + N_{e-e-}, red dashed curve; DWBA, without N_{e-e-}, long solid blue; FBA, dotted green. The momentum transfer direction is indicated by the vertical brown arrow. The experiment is relative and has been normalized to the DWBA to give the best visual fit.

thus incumbent on theory to explore kinematical arrangements where the shape of the TDCS is sensitive to the choice of projectile. With this in mind, we varied the kinematics in our DWBA calculations by changing the value of θ_1. For a scattered angle $\theta_1 = 16^\circ$ we found some interesting differences in the recoil direction between the TDCSs for e^+ and e^-. The cross sections for the three angles are shown in Fig. 7.

Again, PCI has only a small effect in all three cases. The binary peak in the positron case is enhanced over the electron case for $\theta_1 = 2.5^\circ$ and 8° but is smaller for 16°. Furthermore, in the positron case there is a local minimum in the recoil direction which is absent for electron-impact ionization. The relative behavior in the binary direction is an exchange effect and depends on the absence of the g amplitude in the positron case.

In order to better understand this striking difference between the positron and electron results in the recoil direction, in Fig. 7(c) we performed a series of model calculations shown in Fig. 8. The calculations can be summarized as follows:

(i) PWIA: plane waves for all free particles, no exchange amplitude g. This calculation elucidates the contribution of target wave-function effects to the shape of the TDCS.

(ii) FBA: plane wave for incoming and scattered particle, no exchange amplitude g, slow ejected electron calculated in the static potential of ion.

(iii) PWDWPW: plane wave for incoming and fast ejected particle, no exchange amplitude g, singlet static exchange for ejected electron.

(iv) DWBA (electron): spin singlet static exchange for both exiting electrons, slow electron in field of ion, fast electron in field of atom, wave functions of both outgoing particles orthogonalized to ground state.

(v) DWBA (positron): singlet static-exchange potential for ejected electron in field of ion, static atomic potential for

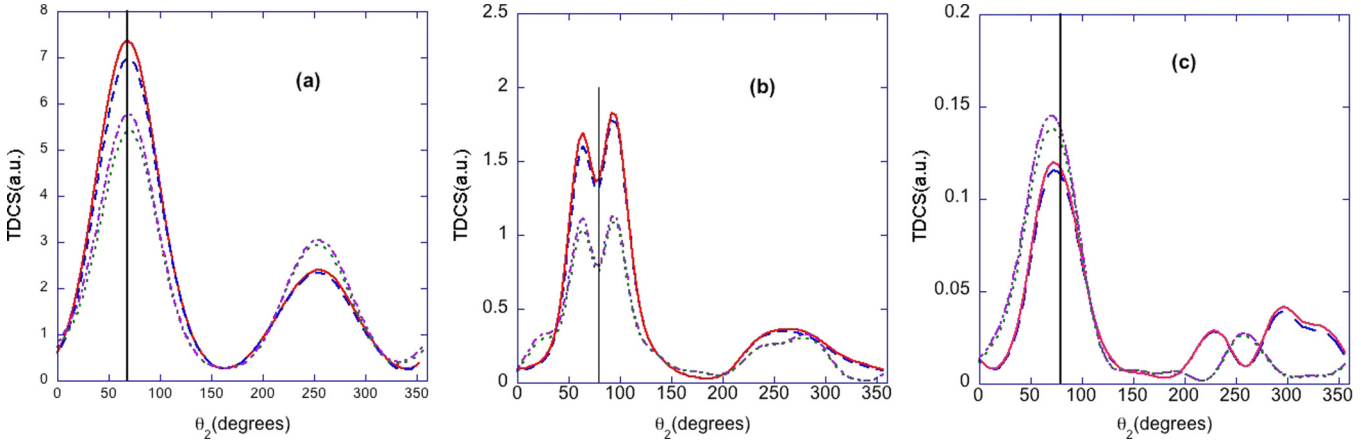

FIG. 7. TDCS for the electron and positron impact ionization of Xe($5p$), $E_0 = 1.0328$ keV, $E_1 = 1$ keV, $E_2 = 20$ eV: (a) $\theta_1 = 2.5^\circ$, (b) $\theta_1 = 8^\circ$, (c) $\theta_1 = 16^\circ$. Electron curves: DWBA + N_{e-e-}, green dotted curve; DWBA without N_{e-e-}, purple dashed dotted. The positron curves are DWBA + N_{e+e-}, solid red; DWBA without pci, long dashed blue. The momentum transfer direction is indicated by the solid vertical line.

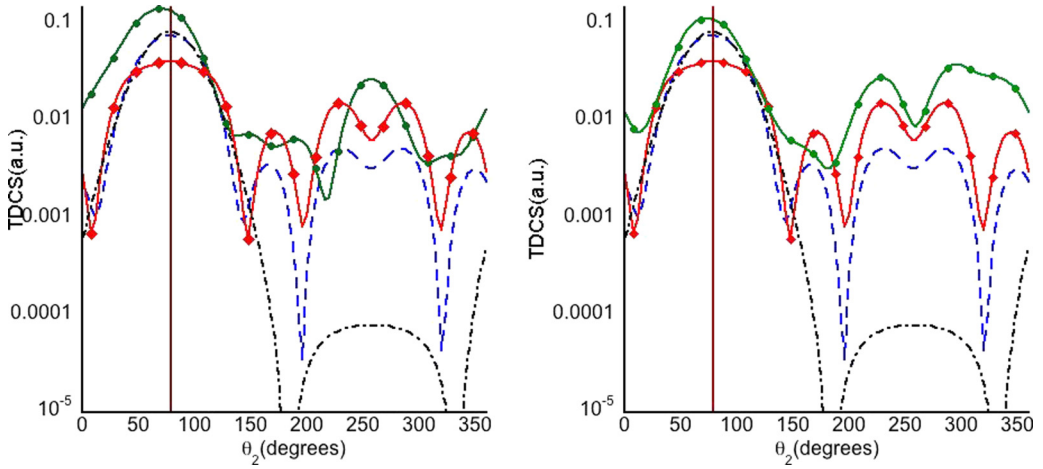

FIG. 8. TDCS for the ionization of Xe($5p$), left panel for electron impact, right panel for positron impact. $E_0 = 1.0328$ keV, $E_1 = 1$ keV, $E_2 = 20$ eV, $\theta_1 = 16^\circ$, all curves without PCI. DWBA, green with filled disks; PWIA, black dashed dotted; FBA, dashed blue, PWDWPW, red with filled diamonds. The brown vertical line shows the direction of momentum transfer.

positron, direct amplitude only, wave function of slow electron orthogonalized to the ground state.

The PWIA is very much smaller than the other cross sections. We see two zeros in the recoil direction. These arise because k_{recoil} passes through the second node of the Xe($5p$) wave function, corresponding to $k_{\text{recoil}} \approx 2.95$ (see Fig. 9).

It appears that the FBA TDCS, though much bigger, retains a "memory" of the zeros in the PWIA. There is in the FBA calculation a local minimum in the recoil peak. This minimum is entirely absent from the PWIA and it is not, therefore, a wave-function effect. The only difference between FBA and PWIA is that the former allows for the elastic scattering of the slow ejected electron and consequently, we conclude that this must be the origin of the local minimum. The PWDWPW differs from the FBA only in the possibility of exchange for the slow ejected electron. The full DWBA calculations are the only ones that differentiate between positron and electron scattering. In the electron case we experimented with "switching off "the exchange potential for the incoming and scattered electron and it made very little difference. We conclude that a major difference between the positron and electron-impact ionization is in the elastic scattering in the incident channel. This might come as something of a surprise, since Rutherford scattering from the nucleus would give rise to an identical elastic differential cross section for both electron and positron scattering. However, it is well known that for scattering from a xenon atom the elastic scattering differential cross section (DCS) is very different for the two particles. In Fig. 10 we show the differential cross section for an impact energy of 1032.8 eV calculated using the accurate *ab initio* optical potential approach of [49]. For

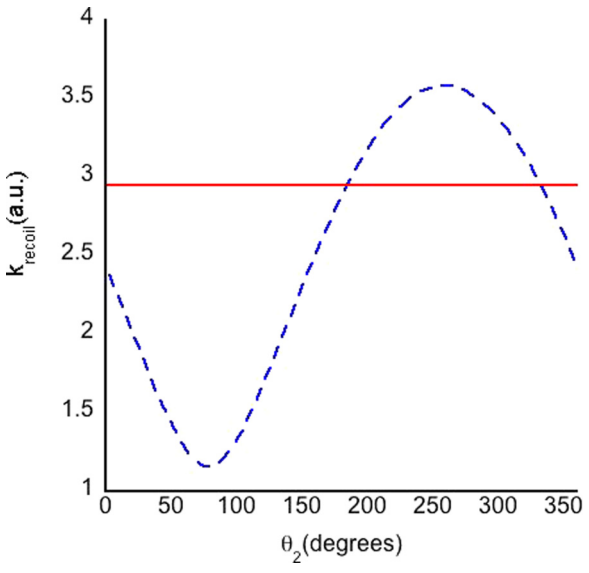

FIG. 9. $k_{\text{recoil}} = |\mathbf{k}_0 - \mathbf{k}_1 - \mathbf{k}_2|$ plotted as a function of θ_2 for Xe($5p$), $E_0 = 1.0328$ keV, $E_1 = 1$ keV, $E_2 = 20$ eV, $\theta_f = 16^\circ$. The horizontal line at 2.95 is the value for the second node in Fig. 2.

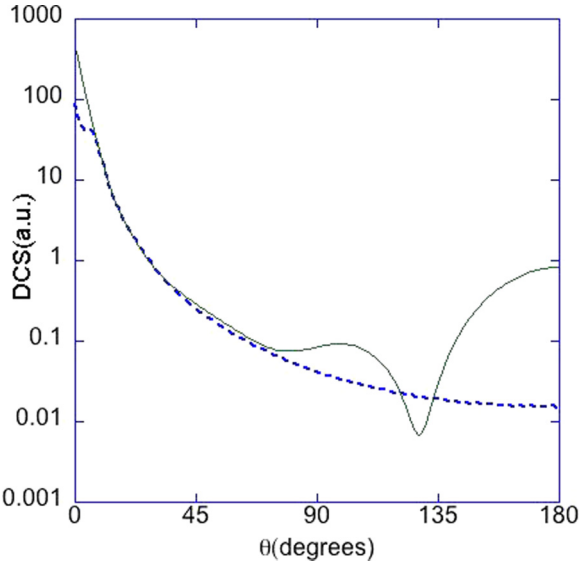

FIG. 10. Elastic differential cross section for electron, solid line, and positron, dashed line, impact on xenon, calculated using the optical potential method of [49]. The projectile impact energy is 1032.8 eV.

very small angles the electron DCS is a factor of 6 larger than that of the positron, while for 180° it is 2 orders of magnitude larger. For electron scattering in coplanar symmetric geometry, a peak at large angles has been observed [50,51] and explained in terms of multiple scattering [15,52]. Because the probability of large-angle scattering of the positron is so much smaller, one would not expect to see a large angle peak in the positron case and indeed, when we performed such calculations none was evident. Equally, one would expect to see a single peak for positron scattering in perpendicular plane geometry, unlike the double peaks predicted and observed in the electron case [15,25,53–55]. For $(e,2e)$ the effect of allowing for the elastic scattering of the fast electron in the final channel leads to the local minimum, seen in the FBA and the PWDWPW, being replaced by a maximum. However, for positron-impact ionization this minimum persists.

V. SUMMARY

Complementary positron- and electron-impact ionization experiments would allow a better understanding of some of the subtleties of few body atomic collision physics. We have presented triple-differential cross sections for the electron-impact ionization of argon($3p$), krypton($4p$), and xenon($5p$), and comparison with experiment is generally encouraging. Agreement with the recent experiments of [3] is less encouraging, but we have argued that since the apparent discrepancy between theory and experiment is seen in both their electron and positron experiments and there is a wealth of evidence that the DWBA performs very well for electron-impact ionization in these kinematics that the problem most likely lies with the measurements. For the xenon($5p$) target in coplanar asymmetric geometry we have confidence in the theoretical description for electron scattering. We have calculated cross sections for both positron and electron scattering in the kinematics of the electron experiments of [20]. We varied the kinematics by changing the angle of the scattered projectile and found an interesting difference between the recoil behavior for positrons and electrons in the recoil direction where $\theta_1 = 16^\circ$ which we attributed to distortion effects, i.e., the elastic scattering of the incident and final particles. Further work would be informative, especially if there were a complementary experimental effort. We recommend the project to our experimental colleagues.

ACKNOWLEDGMENTS

We would like to thank Professor R. P. McEachran for kindly supplying us with the elastic cross-section results used in Fig. 10. We are grateful to Dr. Oscar G. de Lucio for sharing his experimental results with us and to Dr. Lorenzo Avaldi for clarification on his $(e,2e)$ measurements. Support from the Natural Science and Engineering Council of Canada is gratefully acknowledged.

[1] G. Laricchia, S. Armitage, Á. Kövér, and D. J. Murtagh, Adv. At., Mol., Opt. Phys. **56**, 1 (2008).
[2] M. McGovern, D. Assafrão, J. R. Mohallem, Colm T. Whelan, and H. R. J. Walters, Phys. Rev. A **79**, 042707 (2009).
[3] J. Gavin, O. G. deLucio, and R. D. DuBois, Phys. Rev. A **95**, 062703 (2017).
[4] R. D. DuBois, J. Gavin, and O. G. deLucio, J. Phys. Conf. Series **488**, 072004 (2014).
[5] We are using the notation $A(nl)$ to mean the ionization of the n,l electron from atom A. For example, $Ne(2p)$ represents the processes $e^{\pm} + Ne(1s^2,2s^2,2p^6) \rightarrow e^{\pm} + e^{-} + Ne^{+}(1s^2,2s^2,2p^5)$.
[6] A. Kover, G. Laricchia, and M. Charlton, J. Phys. B **26**, L575 (1993).
[7] A. Kover, M. Finch, M. Charlton, and G. Laricchia, J. Phys. B **30**, L507 (1997).
[8] R. A. Sparrow and R. E. Olson, J. Phys. B **27**, 2647 (1994).
[9] R. I. Campeanu and M. Alam, Eur. Phys. J. D **66**, 19 (2012).
[10] R. I. Campeanu, Eur. Phys. J. D **71**, 296 (2017).
[11] Radu I. Campeanu, H. R. J. Walters, and Colm T. Whelan, Eur. Phys. J. D **69**, 235 (2015).
[12] M. Brauner, J. S. Briggs, and H. Klar, J. Phys. B **22**, 2265 (1989).
[13] J. Berakdar and H. Klar, J. Phys. B **26**, 3891 (1993).
[14] F. Navarette, R. Della Picca, J. Fiol, and R. O. Barrachina, J. Phys. B **46**, 115203 (2013).
[15] C. T. Whelan, R. J. Allan, H. R. J. Walters, and X. Zhang, in $(e,2e)$ & *Related Processes*, edited by Colm T. Whelan, H. R. J. Walters, A. Lahmam-Bennani, and H. Ehrhardt (Kluwer, Dordrecht, 1993), pp. 33–74.
[16] L. Avaldi, R. Camilloni, R. Multari, G. Stefani, X. Zhang, H. R. J. Walters, and Colm T. Whelan, Phys. Rev. A **48**, 1195 (1993).
[17] C. T. Whelan, R. J. Allan, and H. R. J. Walters, J. Phys. IV France **3**, C6-39 (1993).
[18] H. R. J. Walters, R. J. Allan, J. Rasch, J. Röder, K. Jung, and H. Ehrhardt, Phys. Rev. A **50**, 4394 (1994).
[19] J. Rasch, Ph.D. thesis, University of Cambridge, 1996.
[20] J. Rasch, M. Zitnik, L. Avaldi, Colm T. Whelan, G. Stefani, R. Camilloni, R. J. Allan, and H. R. J. Walters, Phys. Rev. A **56**, 4644 (1997).
[21] J. Rasch, Colm T. Whelan, R. J. Allan, S. P. Lucey, and H. R. J. Walters, Phys. Rev. A **56**, 1379 (1997).
[22] S. Rioual, B. Rouvello, A. Pochat, J. Rasch, H. R. J. Walters, Colm T. Whelan, and R. J. Allan, J. Phys. B **30**, L475 (1997).
[23] I. Taoiul, A. Duguet, A. Lahmam-Bennani, B. Lohmann, J. Rasch, Colm T. Whelan, and H. R. J. Walters, J. Phys. B **32**, L5 (1999).
[24] C. T. Whelan, in *Fragmentation Processes: Topics in Atomic and Molecular Physics* (Cambridge University Press, Cambridge, 2013), pp. 207–241.
[25] F. K. Miller, Colm T. Whelan, and H. R. J. Walters, Phys. Rev. A **91**, 012706 (2015).
[26] D. H. Madision, R. V. Calhoun, and W. N. Shelton, Phys. Rev. A **16**, 552 (1977).
[27] E. Clementi and C. Roetti, At. Data Nucl. Data Tables **14**, 177 (1974).
[28] J. B. Furness and I. E. Mc Carthy, J. Phys. B **6**, 2280 (1973).
[29] M. E. Riley and D. G. Truhlar, J. Chem. Phys. **63**, 2182 (1975).
[30] J. M. Martinez, H. R. J. Walters, and Colm T. Whelan, J. Phys. B **41**, 065202 (2008).

[31] B. H. Bransden, M. R. C. McDowell, C. J. Noble, and T. Scott, J. Phys. B **9**, 1301 (1976).
[32] E. P. Curran and H. R. J. Walters, J. Phys. B **20**, 337 (1987).
[33] J. Botero and J. H. Macek, Phys. Rev. Lett. **68**, 576 (1992).
[34] M. Brauner and J. S. Briggs, J. Phys. B **19**, L325 (1986).
[35] E. P. Curran, C. T. Whelan, and H. R. J. Walters, J. Phys. B **24**, L19 (1991).
[36] S. P. Lucey, J. Rasch, and C. T. Whelan, Proc. R. Soc. London, Ser. A **455**, 349 (1999).
[37] S. J. Ward and J. H. Macek, Phys. Rev. A **49**, 1049 (1994).
[38] E. Weigold and I. E. McCarthy, *Electron Momentum Spectroscopy* (Kluwer/Plenum, New York, 1999).
[39] H. Bethe, Ann. Physik **397**, 325 (1930).
[40] B. H. Bransden and C. J. Joachain, *Physics of Atoms and Molecules* (Prentice Hall, Harlow, 2003).
[41] C. T. Whelan, Math. Proc. Cambridge Philos. Soc. **95**, 179 (1984).
[42] T. Rösel, J. Röder, L. Frost, K. Jung, H. Ehrhardt, S. Jones, and D. H. Madison, Phys. Rev. A **46**, 2539 (1992).
[43] H. Ehrhardt and T. Rösel, in $(e,2e)$ & *Related Processes*, edited by C. T. Whelan, H. R. J. Walters, A. Lahmam-Bennani, and H. Ehrhardt (Kluwer, Dordrecht, 1993), pp. 76–82.
[44] L. Avaldi, I. E. McCarthy, and G. Stefani, J. Phys. B **22**, 3079 (1989).
[45] A. Naja, E. M. Staicu-Casagrande, X. G. Ren, F. Catoire, A. Lahmam-Bennani, C. Dal Cappello, and C. T. Whelan, J. Phys. B **40**, 2871 (2007).
[46] L. R. Hargreaves, M. A. Stevenson, and B. Lohmann, Meas. Sci. Technol. **21**, 055112 (2010).
[47] M. A. Stevenson and B. Lohmann, Phys. Rev. A **77**, 032708 (2008).
[48] X. Ren *et al.*, Phys. Rev. A **93**, 062704 (2016).
[49] S. Chen, R. P. Mc Eachran, and A. D. Stauffer, J. Phys. B **41**, 025201 (2008).
[50] A. Pochat, R. J. Tweed, J. Peresses, J. Joachain, C. B. Piraux, and F. W. Byron, Jr., J. Phys. B **16**, L775 (1983).
[51] L. Frost, P. Freienstein, and M. Wagner, J. Phys. B **23**, L715 (1990).
[52] X. Zhang, C. T. Whelan, and H. R. J. Walters, J. Phys. B **23**, L509 (1990).
[53] M. B. J. Woolf, Ph.D. thesis, University of Manchester, 1996.
[54] A. J. Murray, *Fragmentation Processes: Topics in Atomic and Molecular Physics*, edited by C. T. Whelan (Cambridge University Press, Cambridge, England, 2013), pp. 164–206.
[55] X. Zhang, C. T. Whelan, and H. R. J. Walters, J. Phys. B **23**, L173 (1990).